Accepted Manuscript

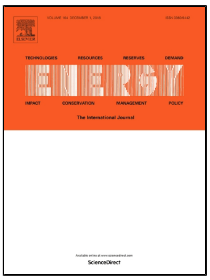

Research on the energy control of a dual-motor hybrid vehicle during engine start-stop process

Xiaolin Tang, Dejiu Zhang, Teng Liu, Amir Khajepour, Haisheng Yu, Hong Wang

PII:	S0360-5442(18)32126-1
DOI:	10.1016/j.energy.2018.10.130
Reference:	EGY 14027
To appear in:	*Energy*
Received Date:	28 July 2018
Accepted Date:	22 October 2018

Please cite this article as: Xiaolin Tang, Dejiu Zhang, Teng Liu, Amir Khajepour, Haisheng Yu, Hong Wang, Research on the energy control of a dual-motor hybrid vehicle during engine start-stop process, *Energy* (2018), doi: 10.1016/j.energy.2018.10.130

Research on the energy control of a dual-motor hybrid vehicle during engine start-stop process

Xiaolin Tang[1,3*], Dejiu Zhang[2], Teng Liu[3*], Amir Khajepour[3], Haisheng Yu[2], Hong Wang[3]

1. State Key Laboratory of Mechanical Transmissions, College of Automotive Engineering, Chongqing University, Chongqing, 400044, P. R. China; 2. School of Mechanical Engineering, Shanghai Jiao Tong University, Shanghai, 200240, P. R.China; 3. Department of Mechanical and Mechatronics Engineering, University of Waterloo, Waterloo, Ontario N2L 3G1, Canada.

*Corresponding author: ***Xiaolin Tang***, Email: tangxl0923@cqu.edu.cn; ***Teng Liu,*** Email: tengliu17@gmail.com.

Abstract: In this paper, motor torque control methods are proposed to suppress the vibration of a dual-motor hybrid powertrain during start-stop operation. Firstly, a co-simulation ADAMS and MATLAB/SIMULINK model is built to study the dynamic characteristics of the hybrid vehicle during modes switching process. Secondly, a torque compensation control method of electric motors is established to compensate the vibration energy source. Thirdly, a vibration transfer path control is built to change the dynamic properties during the engine start-stop process. The results show that the proposed methods can reduce the longitudinal acceleration amplitude of the vehicle to less than 0.4m/s^2, which is only about 30% of the uncontrolled system, during the engine start process. While in the engine stop process, the longitudinal acceleration amplitude of the vehicle is reduced to less than 0.3m/s^2, and the vibration amplitude is only about 20% of the unchanged system. The established methods are effective for suppressing the vehicle vibration and controlling the energy during the modes switching.

Keywords: Energy control, Modes switching, Hybrid vehicle, Two-motor, Vibration control.

1. Introduction

1.1 Motivation and challenge

Due to the depletion of fossil resources and air pollution, many countries have

implemented new standards to restrict vehicles emissions. With their superior emissions and fuel economy performance, hybrid electric vehicles (HEVs) are an effective and common solution to these issues[1-4]. Accordingly, many manufacturers have researched HEV systems and have improved the fuel economy of their vehicles[5-7].

However, in order to achieve better fuel consumption, the hybrid vehicle control system often makes the engine shut down and restart during the switching of hybrid driving mode and pure electric driving mode, leading to serious vibration issues[8-12]. While passengers and drivers are accustomed to conventional vehicle engine shut off (only by turning the ignition key off), hybrid engine start-stop events can be unpredictable, and startling to the driver and passengers. Therefore, generating a smooth transition between the pure electric drive mode and the hybrid driving mode is important, and it is essential to research the transient dynamic behavior of the mode switching and proposed effective measures to suppress the vehicle vibration.

1.2 Literature review

Many researchers have studied vehicle dynamic characteristics during the start and stop processes of the engine. Yoshiaki *et al*.[1] proposed a motor control method to suppress vibration in the Toyota hybrid vehicle during the engine start-stop and rapid acceleration/deceleration processes. In their research, they designed two controllers to reduce the vehicle vibration. The first controller corresponds to the engine torque ripple, and the second controller relates to the torsional vibration of the driveline. Kuang *et al*. [13] investigated the engine start-stop noise and vibration problems in a power-split powertrain. They analyzed the root cause of NVH (Noise, Vibration, and Harshness) problems and proposed measures to resolve them. Affi *et al*. [14] researched the noise and vibration during the engine restart process. Permanently engaged starters and high power starters were proposed and tested to optimize the noise level. Guo *et al*.[15] established a subjective evaluation to diagnose an electric vehicle. They analyzed the interior noise level of the seat track and steering wheel, and measures were chosen to resolve the noise issues. Chen *et al*. [16] established a pulse cancellation algorithm to suppress the desired vibration and smooth ripples of

engine speed during the start-stop process. The simulations showed that the motors can provide torque to suppress the ripple torque with the impletion of the algorithm. Liu *et al*.[17] tested the vibrations of the driver's seat and evaluated them during the engine start. A full-vehicle dynamic model was built to research the countermeasures to reduce the unwanted longitudinal vibration. The research showed that the optimal initial crank angle, the stiffness of damper, and start-up time are limited in their ability to suppress the vehicle vibration. Dinh *et al*.[18] established a simple model to analyze the engine start-stop transient dynamics of a micro/mild hybrid powertrain. They designed a model-based adaptive controller for the engine to crank quickly and smoothly to eliminate the noise, vibration and harshness. The effectiveness of the model and the control approaches were validated by numerical simulations.

1.3 Original contributions

The suppression of vibrations during the engine start-stop process is essential for a power-split hybrid vehicle. The primary objective of this study is to build a co-simulation model and propose effective methods to reduce vibration during the engine starting and stopping phase. There are three original contributions that clearly distinguish this research from the aforementioned studies:

First, a novel dynamic model that is suitable for a power-split hybrid electric vehicle is developed to capture the dynamic properties. The accuracy of this model is verified by a mathematical model of the hybrid powertrain. Based on this dynamic model, a co-simulation ADAMS and MATLAB/SIMULINK model is built to research the dynamic characteristics of the hybrid vehicle during the engine start-stop process.

Second, to prevent engine ripple torque from being transmitted to the hybrid powertrain, an electric motors compensation control method is proposed to compensate the vibration source, which is caused by the compression reaction force and the pumping pressure of the cylinder.

Third, based on a verified and simplified mathematical model of the hybrid powertrain, a vibration transfer path control is built to change the dynamic properties during the engine start-stop process. The research results show that the proposed

methods are effective ways to suppress the vehicle vibration during mode switches.

1.4 Overview

The rest of this paper is organized as follows. The structure of the dual-motor power-split hybrid powertrain is described in Section 2. Section 3 introduces the co-simulation ADAMS and MATLAB/SIMULINK model. In Section 4, two motor control methods are discussed to explore the transient dynamic characteristics of engine start-stop, and the simulation results are provided. Finally, key conclusions are summarized in Section 5.

2. Structure of the dual-motor hybrid system

The full hybrid system[19,20], researched in this paper, is a complicated electromechanical coupling system, as illustrated in Fig.1. This full hybrid electric vehicle is composed of an internal combustion engine, a torsional damper, a compound planetary gear set, electric motors MG1 and MG2, a reducer, a differential, half shafts, and wheels. The compound planetary gear set, as shown in the right part of Fig.1, is comprised of a ring, a carrier, a small sun gear, a large sun gear, three short planets, and three long planets. The engine is a 4-cylinder with the displacement of 1.8 L, the rated power of 93KW, and the maximum speed of 5700rpm. The rated power of MG1 is 42KW, and its maximum speed is 8500rpm, while the rated power of MG2 is 57 KW, and its maximum speed is 8500rpm. The four shafts of the planetary gear set are connected to the engine, MG1, MG2 and output shaft, respectively. The speed of engine is independent from the speed of vehicle. By controlling the rotational speed and torque of the electric motors, the engine can work in the optimal working condition in the hybrid driving mode. Moreover, the continuous various speeds and fuel economy can be achieved and the driving force is guaranteed as well.

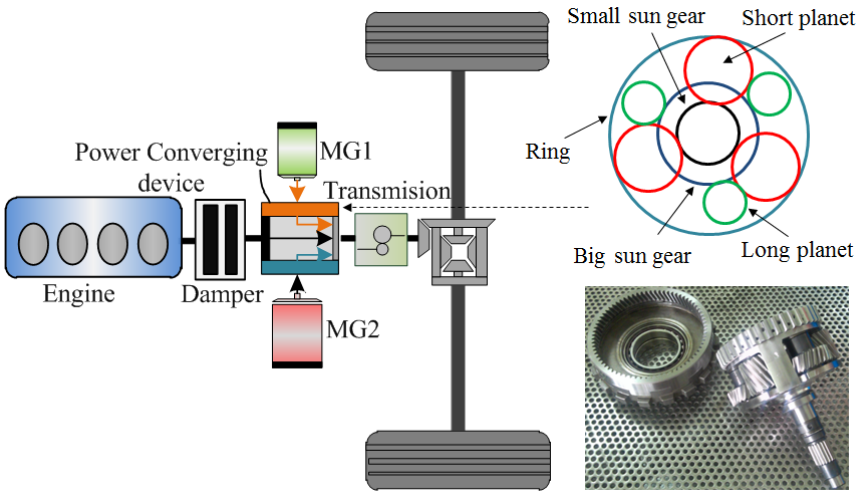

Fig.1 Schematic of the dual motors hybrid electric vehicle.

3. *Dynamic modeling and verification of the hybrid system*

3.1 Dynamic modeling of hybrid vehicle

To investigate the torsional vibration characteristics of the hybrid vehicle, it is important to establish the dynamic model of the hybrid vehicle[21]. The simplified engine model includes the cranks, connecting rods, flywheel, pistons, and cylinders. Fig.2 shows the dynamic models of the planetary gear set.

Fig. 2 Dynamic models of planetary gears.

There are two ways to transmit the torsional vibration from engine to vehicle body. One is the transmission system, and the other one is the engine mounts. In order to analyze the dynamic properties of the vehicle during the engine start-stop, the engine mounts system must be modeled. Table 1 shows the mass and rotational inertia of the powertrain, and Table 2 shows the stiffness of the engine mounts.

Table 1 Mass and rotational inertia of powertrain

Parameters	M(kg)	J_{xx} (kg • m^2)	J_{yy}(kg • m^2)	J_{zz}(kg • m^2)
Value	195.7	14.42	5.911	12.414

Table 2 Mounting component's Stiffness

Mount point	Static stiffness (N/mm)			Dynamic stiffness(N/mm)		
	u_i	v_i	w_i	u_i	v_i	w_i
Top-right point	130	130	177	169	169	230
Top-left point	104	86	271	135	112	352
Front point	202	48	41	263	62	53
Back Point	202	48	41	263	62	53

In this paper, the front suspension is Macpherson suspension and the rear suspension is the Double-wishbone suspension[22]. The Macpherson suspension includes the lower control arm, steering tie rod, steering knuckle assembly, wheel assembly and shock absorber.

Fig.3 shows the full vehicle model of the hybrid system, which includes the engine, transmission system, engine mounting system, suspension system and the vehicle body.

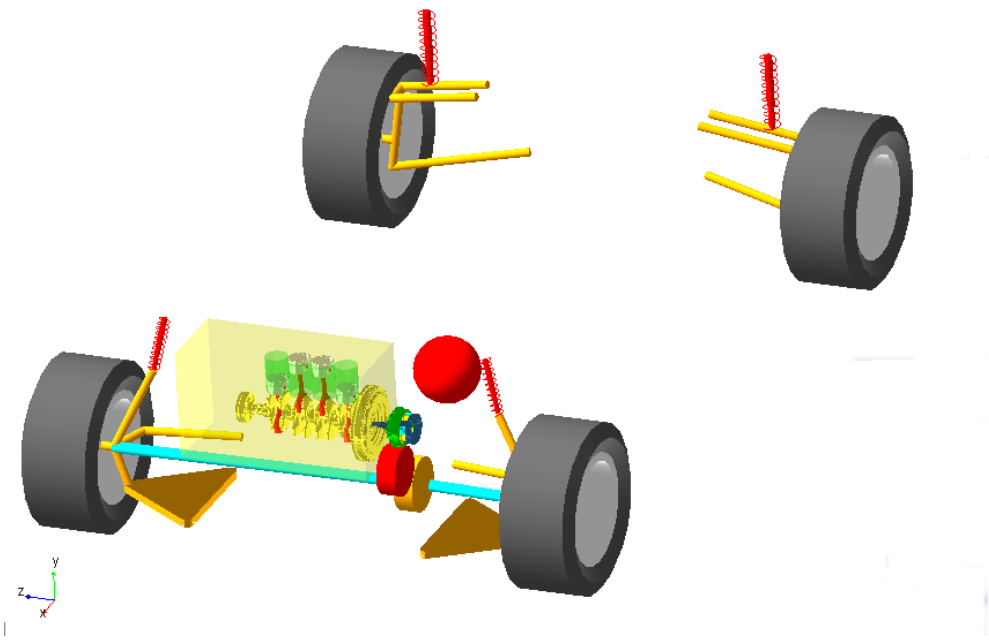

Fig. 3 Full vehicle model in ADAMS.

3.2 Verification of the dynamic model

In order to verify the dynamic model, a 13 degree-of-freedom mathematical model of the hybrid system is built.

The imbalance force and torque fluctuation are the main excitation force of the powertrain. Therefore, when building the vehicle body model, the other directions can be simplified. A 13 degree of freedom model is shown in Fig.7, which contains the vehicle (3 DOF), suspension system(4 DOF) and powertrain (6 DOF).

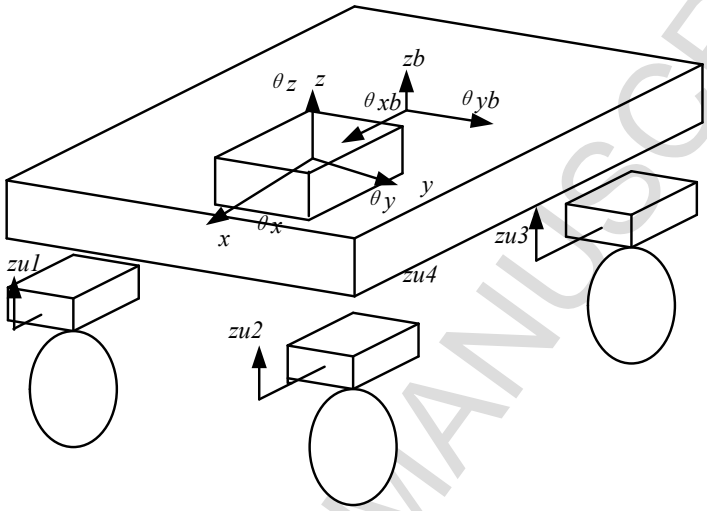

Fig. 4 13DOFs vehicle multi-body dynamics model.

the 13 degree of freedoms can be written as

$$x = \begin{bmatrix} x_1 & x_2 & x_3 \end{bmatrix}^T \tag{1}$$

where the generalized coordinates of the powertrain are described as

$$x_1 = \begin{bmatrix} x & y & z & \theta_x & \theta_y & \theta_z \end{bmatrix}^T \tag{2}$$

$$x_2 = \begin{bmatrix} z_b & \theta_{xb} & \theta_{yb} \end{bmatrix}^T \tag{3}$$

where x_2 is the generalized coordinates of the vehicle body, the generalized coordinates of the unsprung weight can be written as

$$x_3 = \begin{bmatrix} z_{u1} & z_{u2} & z_{u3} & z_{u4} \end{bmatrix}^T \tag{4}$$

According to the Lagrange equation, the dynamic equation of the system can be shown as

$$M'\ddot{x} + C'\dot{x} + K'x = F' \tag{5}$$

the mass matrix of the vehicle can be written as

$$M' = \begin{bmatrix} m & 0 & 0 \\ 0 & m_b & 0 \\ 0 & 0 & m_u \end{bmatrix} \tag{6}$$

the system damping matrix can be shown as

$$C' = \begin{bmatrix} c_{11} & c_{12} & 0 \\ c_{21} & c_{22} & c_{23} \\ 0 & c_{32} & c_{33} \end{bmatrix} \tag{7}$$

the system stiffness matrix can be descripted as

$$K' = \begin{bmatrix} k_{11} & k_{12} & 0 \\ k_{21} & k_{22} & k_{23} \\ 0 & k_{32} & k_{33} \end{bmatrix} \tag{8}$$

Regardless of the road excitation, the external force of the vehicle is the excitation force of the powertrain. For the four-cylinder engine, the main excitation force is the second-order reciprocating inertial force of the piston and the reciprocating mass and the harmonic fluctuation of the crankshaft torque.

$$F' = [F_x \quad 0 \quad F_z \quad M_x \quad M_y \quad M_z \quad 0 \quad \dots \quad 0]^T_{13\times1} \tag{9}$$

Table 3 shows the natural frequencies of the 13 degrees of freedom mathematical model. The first three modes are the roll, vertical and pitch of the vehicle body. The fourth to the eighth and the eleventh modes are the modes of six degrees of freedom of the engine. The ninth and tenth orders are the modes of the front wheels, and the twelfth and thirteenth are the wheel modes.

Table 3 Natural frequency of 13 DOFs vehicle model

Modes	1st	2nd	3rd	4th	5th	6th	7th
Frequency	1.2	1.6	3.3	7.3	8.8	9.7	10.5
Mode shape	Rolling	Vertical	Pitch	X	Z	R_{ZZ}	Y
Mode	8th	9th	10th	11th	12th	13th	
Frequency	13.3	13.7	13.8	14.3	18.0	18.3	
Mode shape	R_{XX}	Front left wheel	Front right wheel	R_{YY}	Rear right wheel	Rea left wheel	

To verify the accuracy of the built dynamic vehicle model, the dynamic response is carried out. When the driving mode of hybrid vehicle is switched from pure electric mode to hybrid mode, the motors drag the engine to the idle speed (1000rpm), and the

engine is ignited. Therefore, 1000 rpm is chose to validate the dynamic model. Moreover, 1400 rpm is chose to verify the model because the engine often charges the battery at this speed. The vertical vibration of the vehicle at 1000rpm and 1400rpm is transformed with Fourier to obtain the resonant frequency, which is compared with the 13 degrees of freedom mathematical model.

Fig.5 shows the Fourier transform of the vertical acceleration response of the engine at 1000rpm. Table 4 summarizes the resonance frequencies and also gives the error compared with the 13 degrees of freedom. As shown in Table 4, the first six frequencies correspond to the powertrain. When the engine speed is 1000rpm, the excitation frequency is 32Hz. Accordingly, the first, second and fourth order excitation frequencies are 16Hz, 32Hz and 64Hz. Therefore, the last frequencies are the first, second and fourth order of excitation.

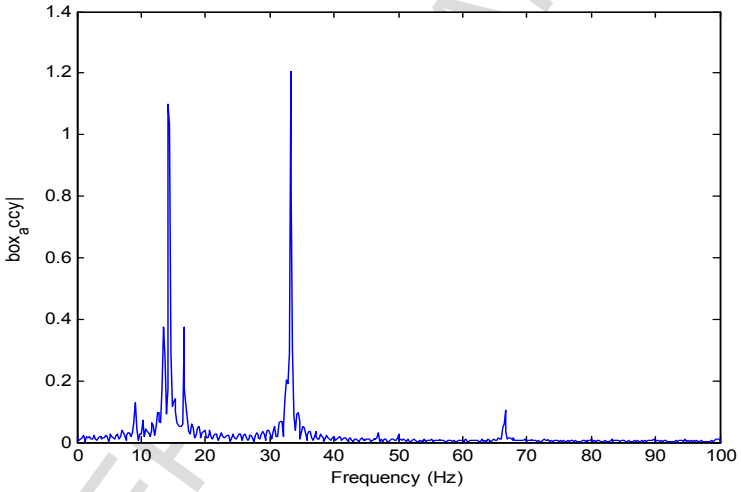

Fig. 5 FFT for the vibration of engine's z origination at 1000rpm.

Table 4 Resonant frequency of the vehicle at engine speed of 1000rpm

Frequency	7.422	9.18	10.16	11.13	13.67	14.26	16.99	33.98	67.97
Mode shape	X	Z	R_{ZZ}	Y	R_{XX}	R_{YY}	First order	Second order	Forth order
Error	1.8%	4.2%	4.7%	5.6%	3.0%	0.2%	6.2%	6.2%	6.2%

Fig.6 shows the Fourier transform of the vertical acceleration response of the engine at 1400rpm. Table 5 summarized the resonance frequencies and also gave the

error compared with the 13 degrees of freedom. Also, the first six frequencies correspond the powertrain, and the last frequencies are the first, second and fourth order of excitation.

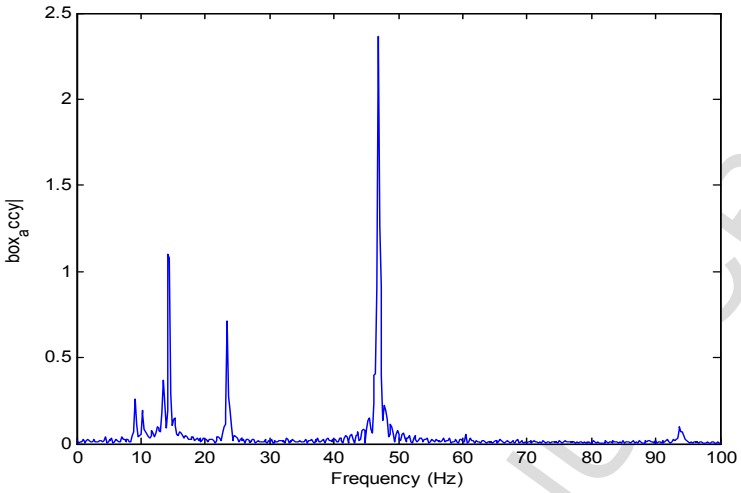

Fig. 6 FFT for the vibration of engine's z origination at 1400rpm.

Table 5 Resonant frequency of the vehicle at engine speed of 1400rpm

Frequency	7.422	9.18	10.16	11.13	13.67	14.45	23.24	46.09	91.19
Mode shape	X	Z	R_{ZZ}	Y	R_{XX}	R_{YY}	First order	Second order	Forth order
Error	1.8%	4.2%	4.7%	5.6%	3.0%	1.1%	3.8%	2.9%	1.8%

For the two conditions of 1000rpm and 1400rpm, the first six frequencies are almost the same, which are the resonant frequencies excited by the engine. The latter three frequencies are the first, second and fourth order of excitation. The first frequency at 1000rpm is 16Hz, and the first frequency at 1400Hz is 22.4 Hz. Compared with the natural frequencies of 13 degrees of freedom (as shown in Table.3), it can be concluded that the dynamic model established by ADAMS can capture the main characteristics of the vehicle.

4. Vibration control of engine start-stop

4.1 Co-simulation of ADAMS and MATLAB/Simulink

4.1.1 Modeling of the control system

According to the connection of the compound planetary gear components, the

speed relationship of the different components can be expressed as

$$n_{PC} = \frac{i_{02} n_{S1} - i_{01} n_{S2}}{i_{02} - i_{01}} \tag{10}$$

$$n_R = \frac{(1 - i_{02})\, n_{S1} - (1 - i_{01})\, n_{S2}}{i_1 - i_2} \tag{11}$$

where n_{pc} is the speed of planetary carrier; n_R is the speed of ring gear; n_{s1} is the speed of small sun gear; n_{s2} is the speed of big sun gear; i_{01} is the gear ratio between the ring gear and small sun gear; i_{02} is the gear ratio between the ring and big sun gear.

According to Eq.(10) and Eq.(11), the speed of the carrier is independent of the speed of the output shaft. Therefore, in the transmission control, by controlling the rotational speed and torque of the electric motors, the continuous various speed of the hybrid system can be realized.

The dynamic equations of the planetary gear set can be written as

$$\begin{aligned} T_{E1} - J_{S1} \cdot \alpha_{S1} &= T_{S1} \\ T_{E2} - J_{S2} \cdot \alpha_{S2} &= T_{S2} \\ T_{Engin} - J_{PC} \cdot \alpha_{PC} &= T_{PC} \\ -T_L - J_R \cdot \alpha_R &= T_R \end{aligned} \tag{12}$$

The torque balance equation of the power-split system can be depicted as

$$\begin{aligned} T_{PC} + T_{S1} + T_{S2} + T_R &= 0 \\ T_R + T_{S1} \cdot i_{01} + T_{S2} \cdot i_{02} &= 0 \end{aligned} \tag{13}$$

The acceleration coordinate equations of the compound planetary gear set are expressed as

$$\begin{aligned} \alpha_{S1} &= \alpha_R \cdot i_{01} + \alpha_{PC} \cdot (1 - i_{01}) \\ \alpha_{S2} &= \alpha_R \cdot i_{02} + \alpha_{PC} \cdot (1 - i_{02}) \end{aligned} \tag{14}$$

where T_{E1} and T_{E2} are the torque of Electric Motor 1 and Electric Motor 2, respectively; T_E is the torque of engine; T_{PC} is the torque of carrier and T_L is the torque of output shaft. It can be concluded from Eq.(14) that the torque of the engine is also independent of the torque of the output shaft. Therefore, the torque of the

output shaft can be controlled by the coordinating control of the torque of E1 and E2.

According to the aforementioned Equations, the system equation can be given as follows

$$\begin{pmatrix} 1 & 0 & -1 & 0 & 0 & 0 & -J_{S1} & 0 \\ 0 & 1 & 0 & -1 & 0 & 0 & 0 & -J_{S2} \\ 0 & 0 & 0 & 0 & 0 & 1 & 0 & 0 \\ 0 & 0 & 0 & 0 & 1 & 0 & 0 & 0 \\ 0 & 0 & 1 & 1 & 1 & 1 & 0 & 0 \\ 0 & 0 & i_{01} & i_{02} & 0 & 1 & 0 & 0 \\ 0 & 0 & 0 & 0 & 0 & 0 & 1 & 0 \\ 0 & 0 & 0 & 0 & 0 & 0 & 0 & 1 \end{pmatrix} \cdot \begin{pmatrix} T_{E1} \\ T_{E2} \\ T_{S1} \\ T_{S2} \\ T_{PC} \\ T_R \\ \alpha_{S1} \\ \alpha_{S2} \end{pmatrix} = \begin{pmatrix} 0 \\ 0 \\ T_L + J_R \alpha_R \\ T_{Engin} - J_{PC} \alpha_{PC} \\ 0 \\ 0 \\ \alpha_R i_{01} + \alpha_{PC}(1 - i_{01}) \\ \alpha_R i_{02} + \alpha_{PC}(1 - i_{02}) \end{pmatrix} \tag{15}$$

where i_{01}, i_{02}, J_{S1}, J_{S2}, J_R, and J_{PC} are known; T_{Engin} and T_L can be calculated by ADAMS, α_R and α_{PC} are the control variable. Accordingly, T_{S1} and T_{S2} will be carried out, and a planetary torque distribution system can be established. Combined with the vehicle model, a co-simulation model can be built.

4.1.2 Simulation of engine start

Fig.7 shows the engine speed during engine start. The engine starting process can be divided into two stages cranking and ignition[1,23]. During the cranking period, pumping resistance and inertial resistance are the main sources of excitation. After ignition, the combustion torque of the engine is much larger than the resistance torque, and the combustion torque is the main source of exciting force.

Fig.7 shows that the engine has obvious speed fluctuation during the cranking process. However, after ignition, the engine speed is relatively stable.

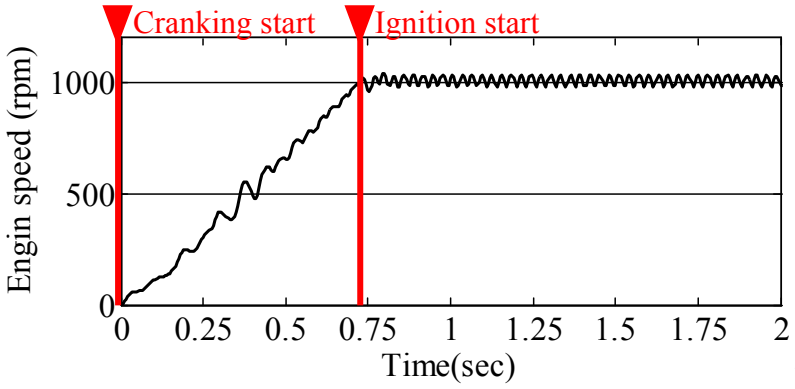

Fig. 7 Crankshaft speed at engine starting stage.

Fig.8 shows the vehicle body acceleration during the cranking process of engine starting. As shown in Fig.8, the fluctuation of the body acceleration occurs during the cranking process, and the maximum acceleration is 1.2m/s^2, which greatly impacts ride comfort, giving drivers a strong sense of insecurity. After the engine is ignited, the vibration of the vehicle is much smaller, and the acceleration amplitude is within 0.3m/s^2, which is in the acceptable range of the driver.

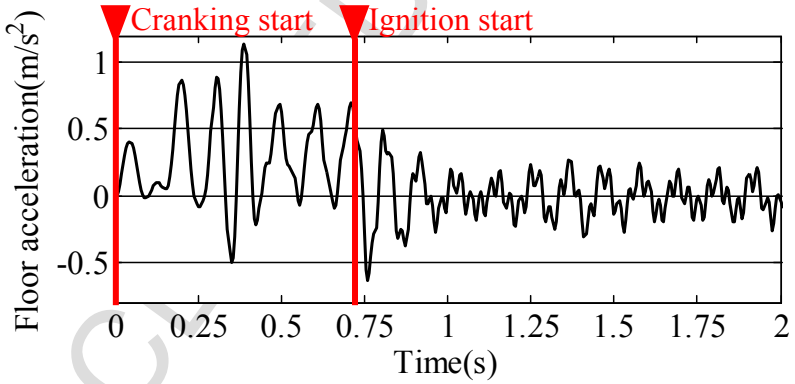

Fig. 8 Longitudinal acceleration of the vehicle at engine starting stage.

4.1.3 Simulation of the engine stop

For hybrid vehicles, switching driving modes leads to frequent starting and stopping of the engine. The engine stopping process also brings unbalanced torque, leading to vibration of the vehicle.

Fig.9 shows the engine speed during the engine stop process. It can be concluded

from Fig.9 that the engine speed is affected by the frictional resistance and finally stops after reaching 0. In this process, the rotational speed of the engine fluctuates, and the rotational speed fluctuates the most at around 400rpm.

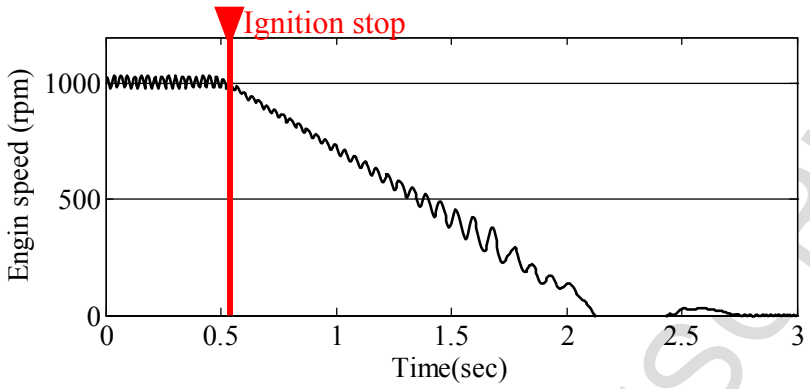

Fig. 9 Crankshaft speed at engine stopping stage.

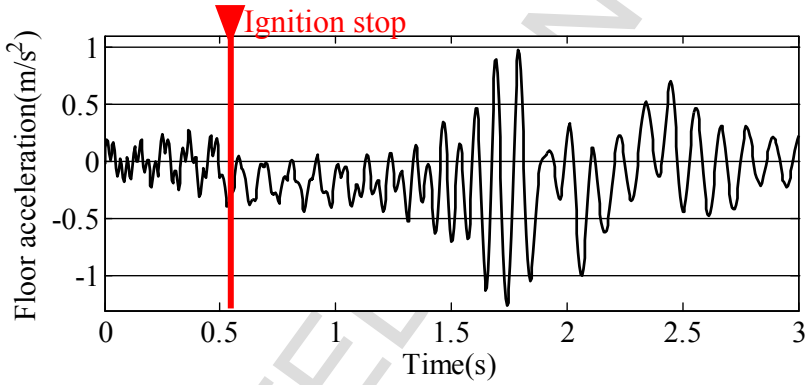

Fig. 10 Longitudinal acceleration of the vehicle at engine stopping stage.

Fig.10 depicts the vehicle acceleration during the engine stop. It can be seen from Fig.11 that while the engine speed decrease, the unbalanced torque is transmitted to the body via the powertrain, which affects the ride comfort of the vehicle body. During this process, the peak acceleration of the vehicle body is 1.3m/s^2，which has an adverse effect on the ride comfort. Moreover, the engine stops frequently during its running, and these vibrations have a great influence on the driver.

4.2 The compensate torque of the engine

As noted previously, the vehicle has the largest vibration amplitude when the engine is not ignited. The pump resistance, inertial resistance, and the frictional resistance bring torque fluctuations, resulting in vehicle impact. Therefore, it is

necessary to calculate the resistance of the engine.

Fig.11 shows the resistance torque of the engine and that there is rapid change near the top dead center (TDC) of the four strokes. This periodical changing torque acts on the flywheel and will lead the vibration of the hybrid powertrain. Therefore, if the unbalanced torque can be compensated by the control of the motor during the start-stop process, the vibration can be solved from the source.

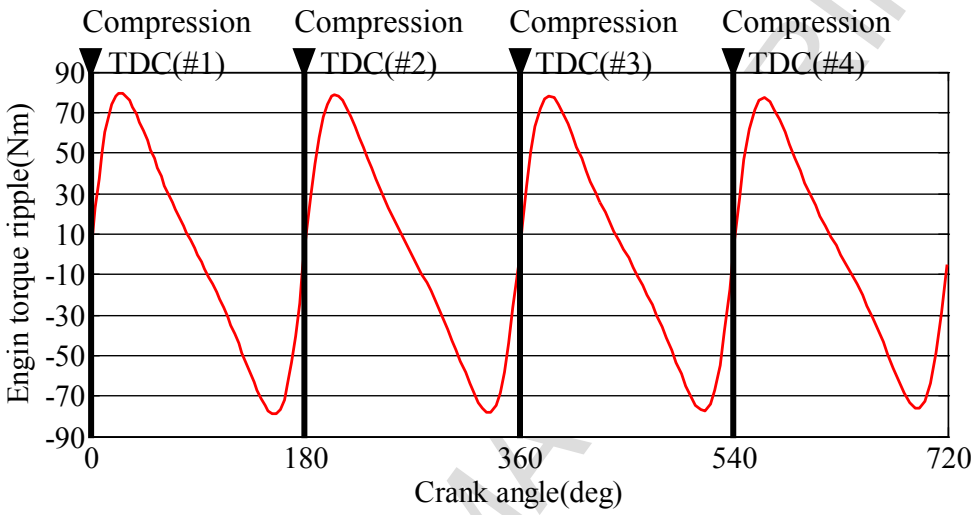

Fig. 11 Engine Torque Ripple.

4.2.1 The compensation of unbalanced engine torque

In the hybrid vehicle, the engine is powered by coordinated control of two motors, and the torques of two motors are distributed according to Eq.(15). The torque compensation is designed to prevent the unbalanced torque of the engine from reaching the vehicle body. Torque of engine includes steady term T_{E_count} and ripple term ΔT_E.

$$T_{Engin} = T_{E\_count} + \Delta T_E \tag{16}$$

To suppress the ripple torque of the engine, additional torques are applied to the small and large motors respectively to realize the compensation control. The torques of motor 1 and motor 2 are expressed as

$$T_{E1} = T_{E1\_ref} + \Delta T_{E1} \tag{17}$$

$$T_{E2} = T_{E2\_ref} + \Delta T_{E2} \tag{18}$$

where T_{E1_ref} and T_{E2_ref} are the compensate torque of motor 1 and motor 2 which are calculated from the steady term of engine torque.

According to the Eq.(12) to Eq.(14), the compensation torque ΔT_{E1} and ΔT_{E2} can be given as follows

$$\Delta T_{E1} = \frac{i_{01}}{i_{01}-i_{02}}\Delta T_E + \frac{1-i_{02}}{i_{01}-i_{02}}T_R + (\frac{1-i_{02}}{i_{01}-i_{02}}J_R + i_{01}J_{s1})\alpha_R + [\frac{i_{02}}{i_{02}-i_{01}}J_{pc} + (1-i_{01})J_{s1}]\alpha_{pc} \tag{19}$$

$$\Delta T_{E2} = -\frac{i_{01}}{i_{01}-i_{02}}\Delta T_E - \frac{1-i_{01}}{i_{01}-i_{02}}T_R + (i_{02}J_{s2} - \frac{1-i_{01}}{i_{01}-i_{02}}J_R)\alpha_R + [\frac{i_{01}}{i_{01}-i_{02}}J_{pc} + (1-i_{02})J_{s2}]\alpha_{pc} \tag{20}$$

4.2.2 Study of engine torque compensation during engine start

Substituting the unbalanced torque of the engine ΔT_E into Eq.(19) and Eq.(20), the compensation torque of two motors can be obtained, respectively. Fig.12 shows the comparisons of motor 1 torque before and after the unbalanced torque compensation. Fig.13 shows the comparisons of motor 2 torque before and after the unbalanced torque compensation. The red line is the motor's torque after compensation and the black line is before compensation.

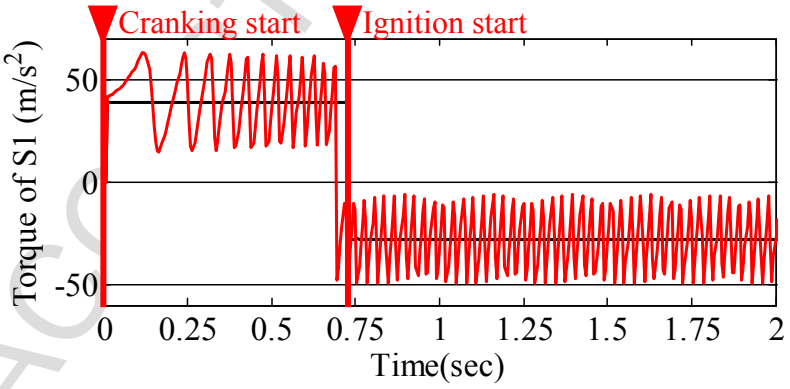

Fig. 12 Torque and compensate of E1.

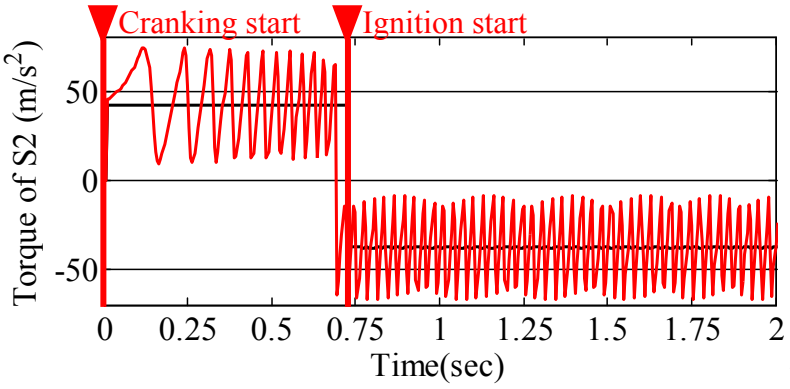

Fig. 13 Torque and compensate of E2.

Fig.14 shows the speed of the engine during the start process before and after unbalanced torque compensation. The red line is the engine speed after compensation and the black line is before compensation. As shown in Fig.14, some unbalanced torque is compensated by motor torque control, and the speed of engine is smoother during the start process. However, some torque fluctuations still exist and impacts the vehicle body.

Fig.15 shows the comparisons of the longitudinal acceleration of the vehicle body before and after unbalanced torque compensation. As shown in Fig.15, the longitudinal vibration of the vehicle is successfully reduced with the the unbalanced torque of the engine compensation. Moreover, the acceleration fluctuation amplitude is reduced to less than 0.7m/s^2, which means that the vehicle vibration is reduced by 40% compared to the uncontrolled manner.

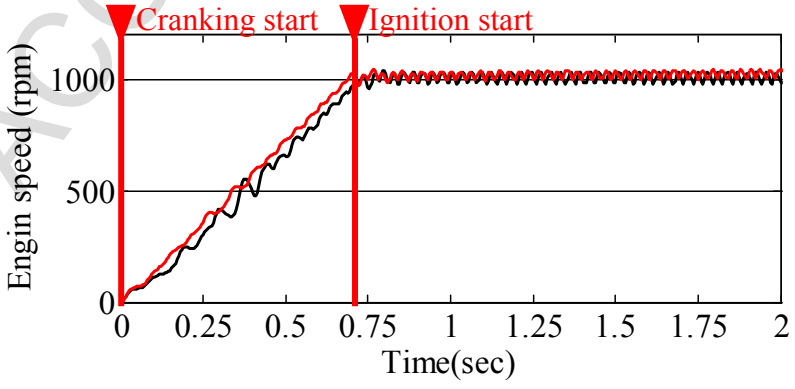

Fig. 14 Engine speed at the starting stage with engine torque compensate.

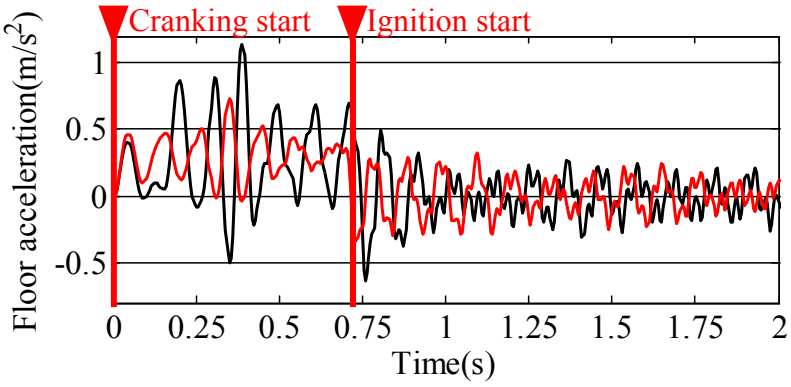

Fig. 15 Longitudinal acceleration of vehicle at the starting stage with engine torque compensate.

4.2.3 Simulation of engine stop process

Fig.16 shows the speed of the engine during the stop process before and after the unbalanced torque compensation. It can be seen from Fig.16 that the fluctuation of the engine speed is obviously reduced with the unbalanced torque of the engine compensation during the engine stop process.

Fig.17 shows the comparisons of the vehicle body's longitudinal acceleration before and after unbalanced torque compensation during the engine stop process. As shown in Fig.17, the longitudinal vibration of the vehicle is successfully reduced with the unbalanced torque of the engine compensation, and the acceleration fluctuation amplitude is reduced to less than 0.5m/s^2, which means that the vehicle vibration is reduced by 60% compared to the uncontrolled manner.

The unbalanced torque compensation control of the engine is more effective in the engine stopping process compared to the engine starting process. The unbalanced torque during the starting and stopping process is equivalent to the sweep signal. The slower the signal passes through the resonance point in the powertrain, the greater the resonance it excites. As the engine stop time is shorter than the engine start cranking time, the vibration induced by the engine stop process is greater than those during the engine start process. After the torque compensation, the vibrations are better suppressed during the stop process than the start process.

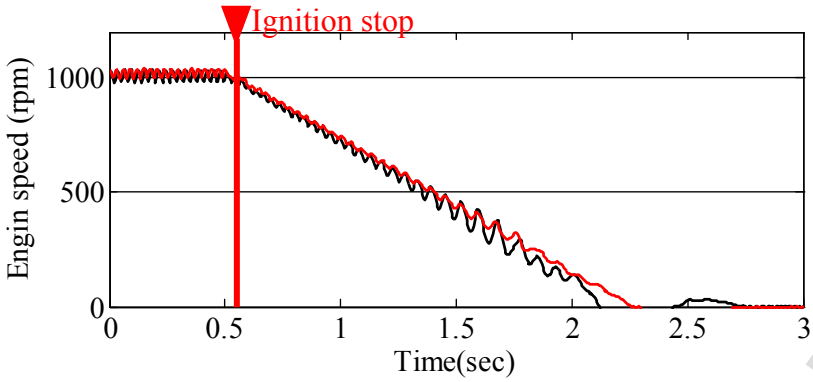

Fig. 16 Engine speed at stopping stage with engine torque compensate

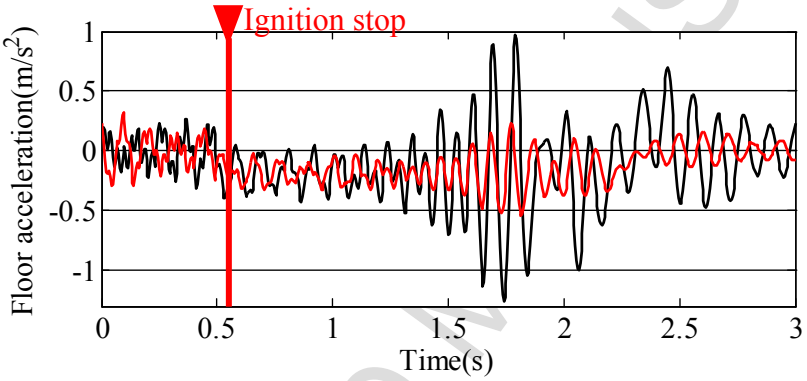

Fig.17 Longitudinal acceleration of the vehicle at stopping stage with engine torque compensate

4.3 Study of vibration transfer path control

4.3.1 Simplification of the hybrid powertrain

The main low natural frequencies of the hybrid system are related to the torsional damper, half-axles, and tires. Moreover, the large torsional stiffness, such as gear meshing, can be simplified to rigid transmission. Therefore, the hybrid system can be approximated by a spring model, where the torsional damper, half-axles, and tires are simplified as torsional springs, as shown in Fig.18.

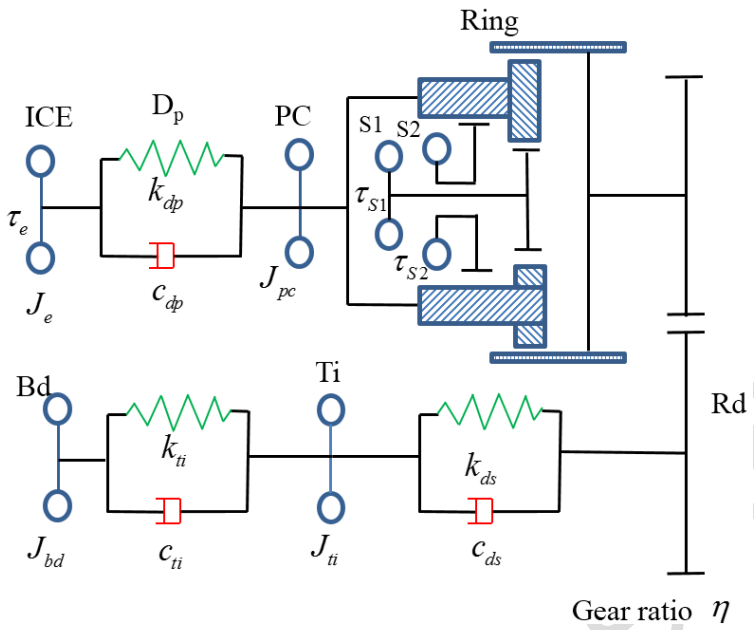

Fig. 18 Simplified Model of Transmission

where J is Inertia moment, k is spring constant, c is damping value, τ is torque, η is the deceleration ratio, *e* is engine, *Dp* is torsional damper, *Pc* is carrier, *S1* is MG 1, *S2* is MG2, *R* is the ring gear, *Rd* is the reduction gear, *Ds* is the drive shaft, *Ti* is the tire, *Bd* is the vehicle body.

In order to change the dynamic properties of the hybrid powertrain, a two-mass simplified model is established to design the controller[20,24], as shown in Fig.19. In the two-mass model, the big sun gear, small sun gear, ring gear and reducer are simplified to the differential. In addition, the tire and vehicle body are simplified to a mass.

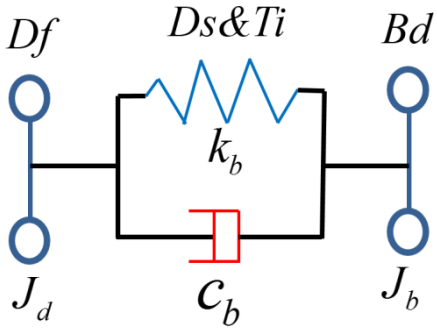

Fig. 19 Two mass model of transmission

where J_d is the equivalent inertia of compound planetary gear set, reducer and

differential, which can be written as

$$J_d = (i_{01}\eta)^2 \cdot J_{S1} + (i_{02}\eta)^2 \cdot J_{S2} + \eta^2 \cdot J_R + \eta_{Rd}^2 \cdot J_{Rd} \tag{21}$$

where i_{01} is the transmission ratio between the small sun gear and ring gear, i_{02} is the transmission ratio between the big sun gear and ring, η is the transmission ratio between the ring and wheel, η_{Rd} is the final deceleration ratio, and J is the inertia of component. J_b is the inertia of wheel and body.

$$J_b = J_{Bd} + J_{Ti} \tag{22}$$

k_b is the equivalent stiffness of the drive shaft and tire

$$\frac{1}{k_b} = \frac{1}{k_{Ds}} + \frac{1}{k_{Ti}} \tag{23}$$

c_b is the equivalent damping of the drive shaft and tire

$$\frac{1}{c_b} = \frac{1}{c_{Ds}} + \frac{1}{c_{Ti}} \tag{24}$$

T is the equivalent torque of differential, θ_d is the angular displacement of differential, and θ_b is the angular displacement of the vehicle body.

4.3.2 Closed-loop control of the two-mass system

The unbalanced torque compensation control of the engine is used to suppress the vehicle vibration from the perspective of the excitation source. However, there are some torque fluctuations still transmitted to the hybrid powertrain. Therefore, based on the control of excitation source, the transmission path of torsional vibration should also be considered to suppress the vibration.

Fig.19 shows the two-mass model of the hybrid powertrain, and its dynamic equation can be written as

$$\left.\begin{aligned} J_d \frac{d^2\theta_d}{dt^2} + c_b(\dot{\theta}_d - \dot{\theta}_b) + k_b(\theta_d - \theta_b) = T \\ J_b \frac{d^2\theta_b}{dt^2} - c_b(\dot{\theta}_d - \dot{\theta}_b) - k_b(\theta_d - \theta_b) = 0 \end{aligned}\right\} \tag{25}$$

where T is the equivalent torque of differential, θ_d is the angular displacement of differential, and θ_b is the angular displacement of the vehicle body.

To establish the state space expression of the system, the state variables must be selected first, and those state variables should be sufficient to fully represent the minimum number of system motion states. For the Equation 25, $\theta_d - \theta_b$ can be taken as a state variable. Accordingly, $x_1 = \dot{\theta}_d$, $x_2 = \dot{\theta}_b$ and $x_3 = \theta_d - \theta_b$ are taken as the state variables. The state space expression can be written as

$$\dot{x} = Ax + BT \tag{26}$$

where, $A = \begin{bmatrix} -\frac{c_b}{J_d} & \frac{c_b}{J_d} & -\frac{k_b}{J_d} \\ \frac{c_b}{J_b} & -\frac{c_b}{J_b} & \frac{k_b}{J_b} \\ 1 & -1 & 0 \end{bmatrix}$, $B = \begin{bmatrix} \frac{1}{J_d} & 0 & 0 \end{bmatrix}^T$.

In order to analyze whether the input variables of the system can fully control the system state and arbitrarily control it from one state to another, it is necessary to determine the controllability of the system. Based on the controllability discriminant matrix, the necessary and sufficient condition for full control is the full rank controllability discriminant matrix.

$$M = \begin{bmatrix} B & AB & A^2B \end{bmatrix} \tag{27}$$

namely

$$rankM = rank\begin{bmatrix} B & AB & A^2B \end{bmatrix} = n \tag{28}$$

as $rank\begin{bmatrix} B & AB & A^2B \end{bmatrix} = 3$, Therefore, the system can be fully controlled.

setting the system output variable is $y = \dot{\theta}_d$, which can be expressed as

$$y = Cx \tag{29}$$

where $C = \begin{bmatrix} 1 & 0 & 0 \end{bmatrix}$.

Therefore, after the Laplace transformation, the transfer function of the system can be expressed as

$$G(s) = C(SI - A)^{-1}B = \frac{\frac{s^2}{J_d} + \frac{c_b}{J_d J_b}s + \frac{k_b}{J_d J_b}}{s(s^2 + c_b(\frac{1}{J_d} + \frac{1}{J_b})s + k_b(\frac{1}{J_d} + \frac{1}{J_b}))} \tag{30}$$

Fig.20 shows the Bode diagram of the system transfer function. It can be concluded from Fig.20 that the resonance peak is 5.44Hz.

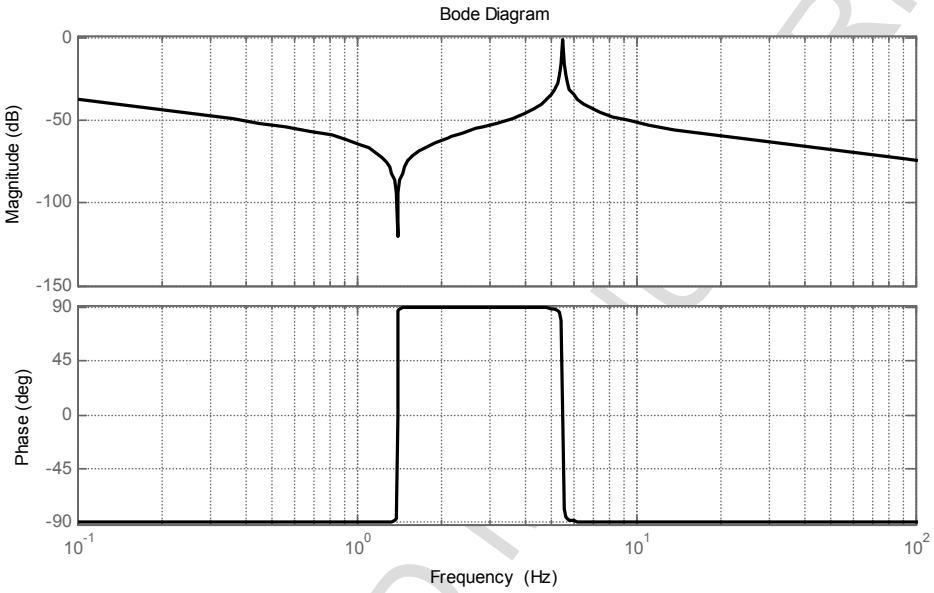

Fig. 20 Bode diagram for the transfer function

In order to reduce the amplitude of the resonant peak, the feedback is introduced and given as follows

$$\Delta T = f(\dot{\theta}_d - \dot{\theta}_b) \tag{31}$$

the input variable after feedback can be written as

$$T' = T - \Delta T = T - f(\dot{\theta}_R - \dot{\theta}_b) \tag{32}$$

Substituting it into Eq.(26), the closed-loop status space is expressed as follows

$$\dot{x} = A'x + BT \tag{33}$$

where $A = \begin{bmatrix} -\frac{c_b}{J_d} - \frac{f}{J_d} & \frac{c_b}{J_d} + \frac{f}{J_d} & -\frac{k_b}{J_d} \\ \frac{c_b}{J_b} & -\frac{c_b}{J_b} & \frac{k_b}{J_b} \\ 1 & -1 & 0 \end{bmatrix}$

the transfer function can be written as

$$G'(s) = C(SI - A')^{-1} B = \frac{\frac{s^2}{J_d} + \frac{c_b}{J_d J_b} s + \frac{k_b}{J_d J_b}}{s(s^2 + c_b(\frac{1}{J_d} + \frac{1}{J_b} + \frac{f}{J_d})s + k_b(\frac{1}{J_d} + \frac{1}{J_b}))} \tag{34}$$

Fig.21 shows the closed-loop Bode diagram of the system. It can be seen from Fig.21 that the feedback control can be used to reduce the resonance peak of the system.

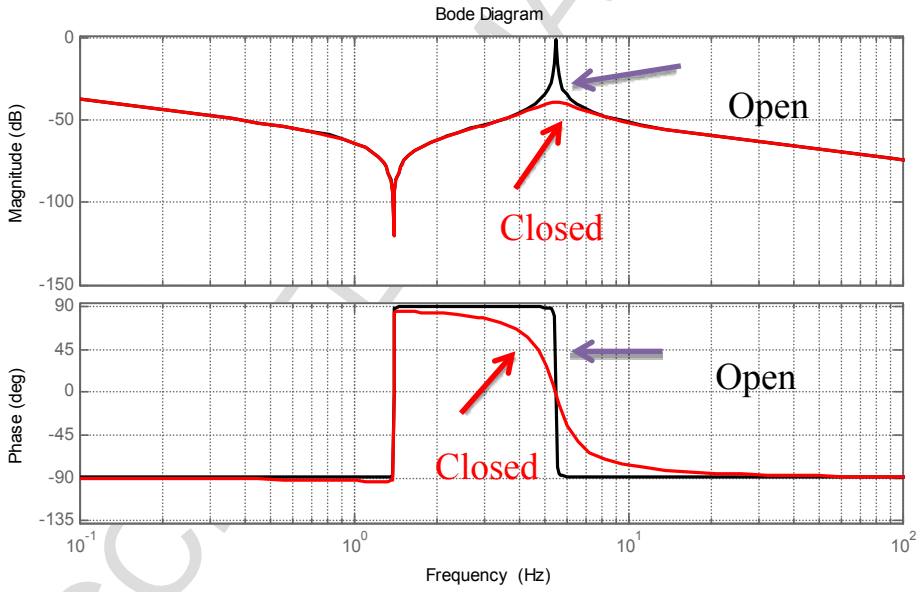

Fig. 21 Bode diagram for the closed loop transfer function

4.3.3 Selection of loop gain

Through the closed-loop feedback control, the resonance peak of the system can be reduced. However, the two-mass powertrain must be dynamic, i.e. when the power-split gives a torque, the system should output the acceleration response accurately and on time.

Eq.(34) shows the transfer function between acceleration and torque, which is given as follows

$$G_\alpha(s)=\frac{\alpha(s)}{T(s)}=sG(s)=\frac{\frac{s^2}{J_d}+\frac{c_b}{J_dJ_b}s+\frac{k_b}{J_dJ_b}}{s^2+c_b(\frac{1}{J_d}+\frac{1}{J_b}+\frac{f}{J_d})s+k_b(\frac{1}{J_d}+\frac{1}{J_b})} \tag{35}$$

As shown in Eq.(35), the acceleration response transfer function is a second-order system.

The transient response properties of the closed-loop control system are determined by the closed-loop poles. Fig.22 shows the root trajectory of the acceleration response transfer function. It can be concluded from Fig.22 that when the gain f is 0, the two poles of the system are two conjugate complex roots close to the imaginary axis. As the gain f increases, the two poles gradually move away from the imaginary axis and move toward the real axis and finally form a pair of double roots on the real axis. As the gain f increases further, one pole moves toward infinity and the other moves toward the original point.

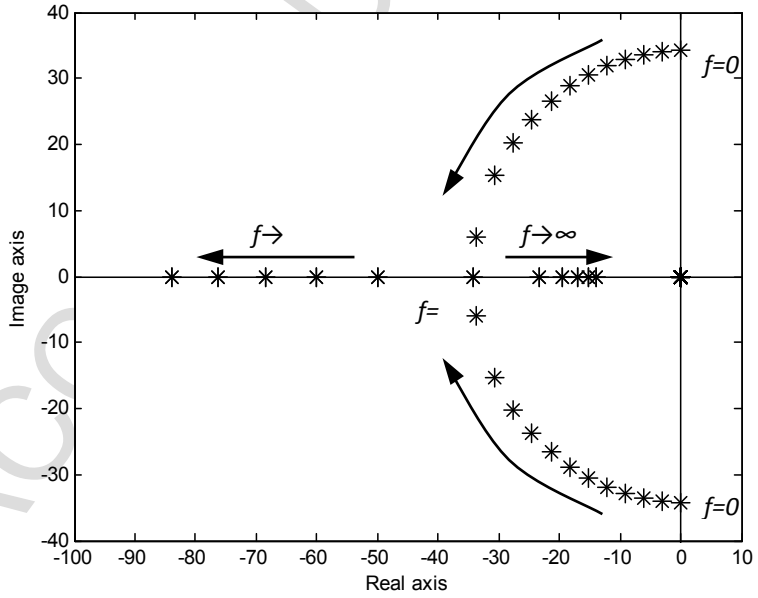

Fig. 22 Root locus of the system

The overshoot M_p, adjustment times and steady state errors are used to describe the

characteristics of the control system. Fig.23 and Fig.24 show the overshoot and adjustment of the two-order control system. It can be seen that the closer the *Mp* line is to the real axis, the smaller the overshoot is; and the farther away the imaginary axis is from the *Ts*, the smaller the adjustment time. In order to restrict the overshoot M_p and reduce the adjustment time, the dominant pole should be closer to the real axis and further away from the imaginary axis. After the optimal design of overshoot and adjustment time, the transient responses of the system accelerations meet the design requirements

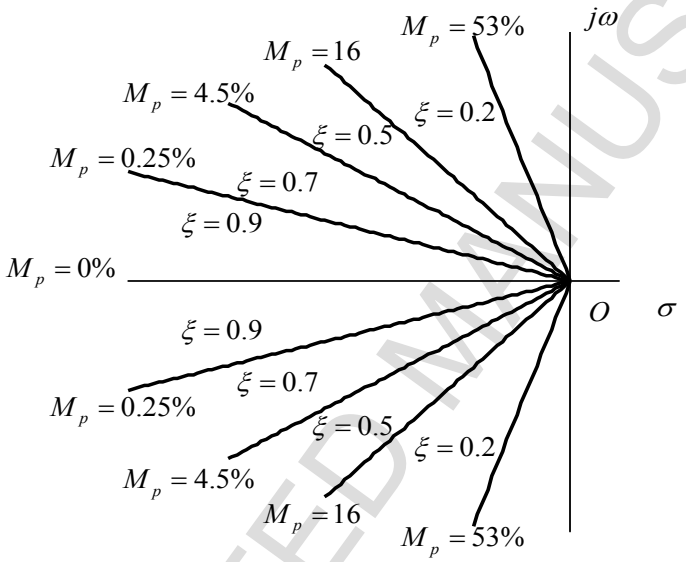

Fig. 23 Root locus Contour lines of M_p

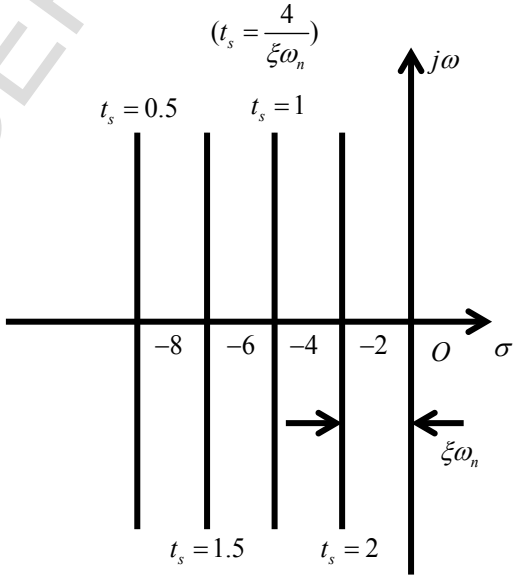

Fig. 24 Root locus Contour lines of t_s

4.3.4 Closed-loop simulation of engine start

In the control step, the feedback amount ΔT is fed back to the equivalent torque of the differential, and this torque needs to be provided by the motors. The equivalent torque on the ring gear can be calculated as:

$$T_R = \frac{T}{\eta} \tag{36}$$

where η is the final ratio, accordingly, the torque will be distributed to the two motors coordinately.

Fig.25 and Fig.26 show the engine speed and vehicle acceleration under closed-loop control during the engine start process, respectively. As shown in Fig.25 and Fig.26, the engine speed is more stable in the closed-loop system. Moreover, the longitudinal acceleration amplitude of the vehicle is reduced to less than 0.4m/s^2, and the vibration amplitude is only about 30% of the uncontrolled system, which is within the acceptable range of the driver.

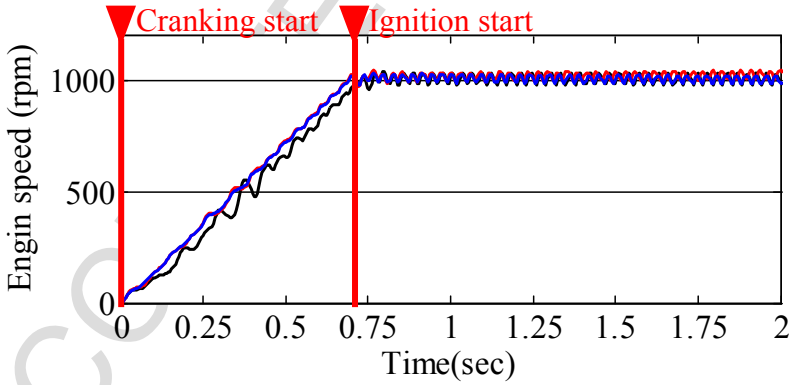

Fig. 25 Engine speed at the starting stage of the closed loop

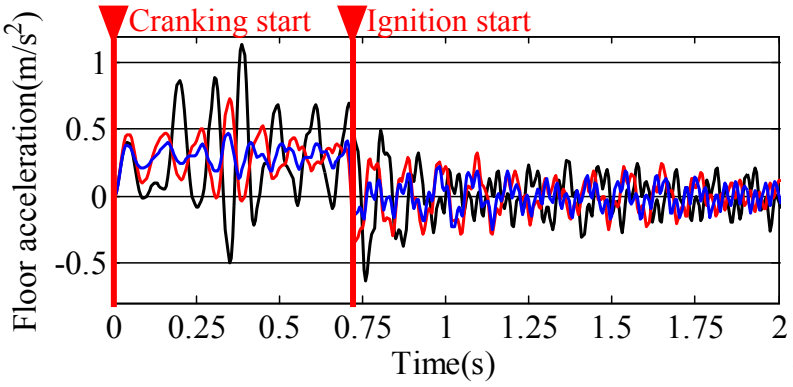

Fig. 26 Longitudinal acceleration of the vehicle at the starting stage of the closed loop

4.3.5 Closed-loop simulation of engine stop process

Fig.27 and Fig.28 show the engine speed and vehicle acceleration, respectively, under closed-loop control during the engine stop process. As shown form Fig.27 and Fig.28, the engine speed is more stable in the closed-loop system. Moreover, the longitudinal acceleration amplitude of the vehicle is reduced to less than 0.3m/s^2, and the vibration amplitude is only about 20% of the uncontrolled system, which is within the acceptable range of the driver.

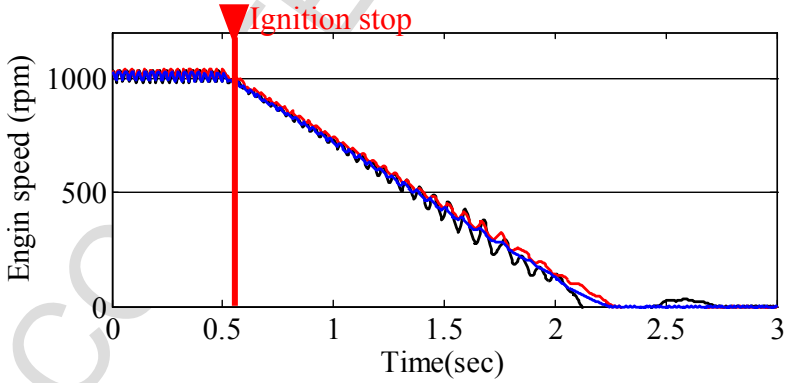

Fig. 27 Engine speed at stopping stage of the closed loop

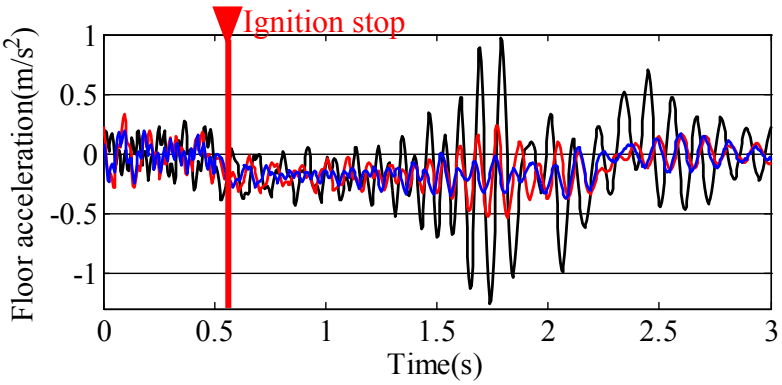

Fig. 28 Longitudinal acceleration of the vehicle at the stopping stage of the closed loop

5. Conclusions

In this paper, a co-simulation ADAMS and MATLAB/SIMULINK model was built to study the dynamic characteristics of a dual-motor hybrid vehicle during the engine start-stop process.

The dynamic equations of this hybrid powertrain were established to control the output torques of the engine and planetary gear set. Based on the so-simulation model and the dynamic equations, the unbalanced torque compensation control of the engine and the torsional vibration control of the powertrain were proposed to suppress the vibration of the vehicle when switching driving modes. The results demonstrated that two methods, vibration source control and vibration transfer path control, were effective to suppress the vehicle vibration during the modes switching. This paper is a useful reference for suppressing engine start-stop vibration.

Acknowledgement

This project is supported by National Natural Science Foundation of China (Grant No. 51705044 and 51575064). The authors would also like to sincerely acknowledge the important support and help from Prof. Jianwu Zhang, Shanghai Jiao Tong University, China.

References

1. Y. Ito, S. Tomura, K. Moriya, Vibration-reducing motor control for hybrid vehicles, R&D Review of Toyota CRDL. 40 (2) (2005) 37-43.
2. H. Khayyam, A. Bab-Hadiashar, Adaptive intelligent energy management system of plug-in hybrid electric vehicle, Energy. 69 (2014) 319-335.
3. F. Millo, C. Cubito, L. Rolando, et al., Design and development of a hybrid light commercial vehicle, Energy. 136 (2017) 90-99.
4. Y. Huang, A. Khajepour, T. Zhu, et al., A Supervisory Energy-Saving Controller for a Novel Anti-Idling System of Service Vehicles, IEEE/ASME Transactions on Mechatronics. 22 (2) (2017) 1037-1046.
5. C. Zou, X. Hu, Z. Wei, and X Tang. Electrothermal dynamics-conscious lithium-ion battery cell-level charging management via state-monitored predictive control. Energy, 141 (2018) 250-259.
6. T. Liu, X. Hu, S. Li, D. Cao, Reinforcement learning optimized look-ahead energy management of a parallel hybrid electric vehicle, IEEE/ASME Transactions on Mechatronics. 22 (4) (2017) 1497-1507.
7. X. Hu, H. Wang, X. Tang, Cyber-physical control for energy-saving vehicle following with connectivity, IEEE Transactions on Industrial Electronics. 64 (11) (2017) 8578-8587.
8. H. Guo, C. Shen, H. Zhang, et al., Simultaneous Trajectory Planning and Tracking Using an MPC Method for Cyber-Physical Systems: A Case Study of Obstacle Avoidance for an Intelligent Vehicle, IEEE Transactions on Industrial Informatics. 2018.
9. C. Hu, R. Wang, F. Yan, et al., Differential steering based yaw stabilization using ISMC for independently actuated electric vehicles, IEEE Transactions on Intelligent Transportation Systems. 19 (2) (2018) 627-638.
10. Y. Qin, C. He, X. Shao, et al., Vibration Mitigation for In-wheel Switched Reluctance Motor Driven Electric Vehicle with Dynamic Vibration Absorbing Structures, Journal of Sound and Vibration. 419 (2018) 249-267.
11. X. Tang, W. Yang, X. Hu, et al., A novel simplified model for torsional vibration analysis of a series-parallel hybrid electric vehicle, Mechanical Systems and Signal Processing. 85 (2017) 329-338.
12. W. Yang, X. Tang, Modelling and modal analysis of a hoist equipped with two-stage planetary gear transmission system, Proc IME K J Multi-body Dynamics. 231(4) (2017)739-749.
13. M. L. Kuang, An investigation of engine start-stop NVH in a power split powertrain hybrid electric vehicle, No. 2006-01-1500. SAE Technical Paper, 2006.
14. A. Sameh, NVH Study of Stop & Start System and Optimized Solutions for Hybrid Vehicles. No. 2014-01-2068. SAE Technical Paper, 2014.
15. R. Guo, Y. Mi, and C. Cao, Subjective and Objective Evaluation of APU Start-Stop NVH for a Range-Extended Electric Vehicle, SAE Technical Paper. 2015-01-0047, 2015, doi:10.4271/2015-01-0047.
16. J. Chen, H. Hwang, Engine automatic start–stop dynamic analysis and vibration reduction for a two-mode hybrid vehicle, Proceedings of the Institution of Mechanical Engineers, Part D: Journal of Automobile Engineering. 227 (9) (2013) 1303-1312.
17. D. Liu, J. Zhang, D. Zhang, et al., Experimental and numerical analysis of the seat track vibrations caused by engine starts in a power-split hybrid electric vehicle, Proceedings of the Institution of Mechanical Engineers, Part D: Journal of Automobile Engineering. 231(3)

(2017) 395-404.

18. T. Dinh, J. Marco, D. Greenwood, et al., Powertrain modelling for engine stop–start dynamics and control of micro/mild hybrid construction machines, Proceedings of the Institution of Mechanical Engineers, Part K: Journal of Multi-body Dynamics. 231(3) (2017) 439-456.
19. X. Tang, X. Hu, W. Yang, et al., Novel Torsional Vibration Modeling and Assessment of a Power-Split Hybrid Electric Vehicle Equipped with a Dual Mass Flywheel, IEEE Transactions on Vehicle Technology. 67(3) (2018) 1990-2000.
20. X. Tang, W. Yang, D. Zhang, H. Yu. A novel two degree of freedom model of a full hybrid electric vehicle, Int. J. Electric and Hybrid Vehicles. 9(1) (2017) 67-77.
21. T. Liu, X. Hu, A bi-level control for energy efficiency improvement of a hybrid tracked vehicle. IEEE Transactions on Industrial Informatics. 14(4) (2018) 1616-1625.
22. Y. Qin, C. Xiang, Z. Wang, et al., Road excitation classification for semi-active suspension system based on system response, Journal of vibration and control. 24(13) (2018) 2732-2748.
23. D Zhang, H Yu, J Zhang, T Lu, X Tang. Analysis and control of torsional vibration in HEV. Drive system technique. 28(4) (2014)3-8. (In Chinese).
24. X. Tang, L. Zou, W. Yang, Y. Huang, H. Wang. Novel mathematical modelling methods of comprehensive mesh stiffness for spur and helical gears. Applied Mathematical Modelling, 64(2018)524-540.

1. A co-simulation ADAMS and MATLAB/SIMULINK model of a dual-motor is built and verified.
2. A torque compensation control method is established to compensate the vibration energy source.
3. A vibration transfer path control is built to suppress the vibration during the engine start-stop process.
4. The proposed methods are effective for suppressing the vehicle vibration and during the modes switching.